

Water Resources Research

RESEARCH ARTICLE

10.1029/2020WR028362

A Framework for Untangling Transient Groundwater Mixing and Travel Times



Key Points:

- We introduce a framework to estimate mean travel times of a groundwater fraction consisting of recently infiltrated river water (F_{rw})
- We test the influence of temporally variable end-member tracer concentrations on estimated mixing ratios
- We demonstrate that the streambed has a major control on the travel times of F_{rw}

Andrea L. Popp^{1,2,3,4} , Álvaro Pardo-Álvarez³ , Oliver S. Schilling^{3,5} ,
 Andreas Scheidegger¹ , Stéphanie Musy⁶ , Morgan Peel³, Philip Brunner³ ,
 Roland Purtschert⁶ , Daniel Hunkeler³ , and Rolf Kipfer^{1,2,7}

¹Eawag, Swiss Federal Institute of Aquatic Science and Technology, Dübendorf, Switzerland, ²Department of Environmental Systems Science, ETH Zurich, Zurich, Switzerland, ³Centre d'Hydrogéologie et de Géothermie, University of Neuchâtel, Neuchâtel, Switzerland, ⁴Now at Department of Geosciences, University of Oslo, Oslo, Norway, ⁵Département de géologie et de génie géologique, Université Laval, Quebec City, Canada, ⁶Climate and Environmental Physics, University of Bern, Bern, Switzerland, ⁷Department of Earth Sciences, ETH Zurich, Zurich, Switzerland

Supporting Information:

- Supporting Information S1

Correspondence to:

A. L. Popp,
andrea.popp@geo.uio.no

Citation:

Popp, A. L., Pardo-Álvarez, Á., Schilling, O. S., Scheidegger, A., Musy, S., Peel, M., et al. (2021). A framework for untangling transient groundwater mixing and travel times. *Water Resources Research*, 57, e2020WR028362. <https://doi.org/10.1029/2020WR028362>

Received 11 JUL 2020
 Accepted 22 FEB 2021

Abstract Understanding the mixing between surface water and groundwater as well as groundwater travel times in vulnerable aquifers is crucial to sustaining a safe water supply. Age dating tracers used to infer apparent travel times typically refer to the entire groundwater sample. A groundwater sample, however, consists of a mixture of waters with a distribution of travel times. Age dating tracers only reflect the proportion of the water that is under the dating range of the used tracer, thus their interpretation is typically biased. Additionally, end-member mixing models are subject to various sources of uncertainties, which are typically neglected. In this study, we introduce a new framework that untangles groundwater mixing ratios and travel times using a novel combination of in-situ noble gas analyses. We applied this approach during a groundwater pumping test carried out in a pre-alpine Swiss valley. First, we calculated transient mixing ratios between recently infiltrated river water and regional groundwater present in a wellfield, using helium-4 concentrations combined with a Bayesian end-member mixing model. Having identified the groundwater fraction of recently infiltrated river water (F_{rw}) consequently allowed us to infer the travel times from the river to the wellfield, estimated based on radon-222 activities of F_{rw} . Furthermore, we compared tracer-based estimates of F_{rw} with results from a calibrated numerical model. We demonstrate (i) that partitioning of major water sources enables a meaningful interpretation of an age dating tracer of the water fraction of interest and (ii) that the streambed has a major control on the estimated travel times.

1. Introduction

Climate change is anticipated to alter the seasonality and quantity of water resources in mountainous regions (e.g., Hock et al., 2019) by affecting snow cover dynamics (e.g., Fiddes et al., 2019), glacier melt (e.g., Huss & Hock, 2015), groundwater storage (Cochand et al., 2019), and river discharge (e.g., Addor et al., 2014; Blöschl et al., 2019; Michel et al., 2020). Although these changes will profoundly influence groundwater recharge and discharge in mountainous environments (Hayashi, 2019), they have largely been ignored so far (Somers et al., 2019). Since surface water and groundwater resources are closely coupled, an improved understanding of surface water-groundwater interactions is highly relevant for a sustainable water governance as well as for water-dependent ecosystems in mountainous regions (e.g., Holman, 2006; Krause et al., 2014; Schilling et al., 2020).

Within the last two decades, studies on river-aquifer exchange dynamics have substantially improved the understanding of the drivers (e.g., river discharge) and controls (e.g., riverbed hydraulic conductivity) of water exchange patterns and their impact on biogeochemical cycling of solutes (e.g., reviews by Boano et al., 2014; Brunner et al., 2017; Lewandowski et al., 2019 and references therein). Particularly, the continued recognition and investigation of riverbed dynamics as key controls on river-aquifer exchange have brought substantial scientific progress in the field of surface water-groundwater interactions (e.g., Mutiti & Levy, 2010; Tang et al., 2018). However, the spatiotemporal dynamics of surface water-groundwater interactions still remain elusive, mainly due to a lack of high-resolution field data (Barthel & Banzhaf, 2016; Boano

© 2021 The Authors.

This is an open access article under the terms of the [Creative Commons Attribution-NonCommercial License](https://creativecommons.org/licenses/by-nc/4.0/), which permits use, distribution and reproduction in any medium, provided the original work is properly cited and is not used for commercial purposes.

et al., 2014; Brunner et al., 2017; Krause et al., 2014; Partington et al., 2017). Consequently, further progress for an improved conceptual understanding as well as model development (which depends on high-resolution field data for model calibration and validation) is limited by the quantity and quality of data available (e.g., Barthel & Banzhaf, 2016; Paniconi & Putti, 2015; Schilling, Cook, & Brunner, 2019).

Environmental tracers such as stable water isotopes or dissolved noble gases have been proven to be highly beneficial to study groundwater flow paths, travel times, and water source partitioning. These tracers deliver an integrated signal over the entire catchment and thus carry important information on water flow paths on large scales (Cook & Herczeg, 2000; Jasechko, 2019; Sprenger et al., 2019 and references therein). Therefore, recent review papers (Brunner et al., 2017; Jasechko, 2019; Schilling, Cook, & Brunner, 2019; Sprenger et al., 2019) emphasize the need for novel, more efficient (isotope) tracer measurement techniques to enhance the understanding of complex feedback mechanisms occurring in river-aquifer systems. Fortunately, recent advances in tracer-based hydrological modeling (e.g., Schilling et al., 2017) have proceeded synchronously with rapid methodological developments in tracer hydrology (Brunner et al., 2017; Paniconi & Putti, 2015)—the latter allowing for high-resolution (e.g., multiple measurements per hour), on-site sampling of stable water isotopes (e.g., Herbstritt et al., 2019; Von Freyberg et al., 2017) or dissolved noble gases (e.g., Mächler et al., 2012). One such technique enabling high-resolution (noble) gas analysis is a recently developed Gas Equilibrium-Membrane Inlet Mass Spectrometer (GE-MIMS; Brennwald et al., 2016) system, which can analyze a multitude of reactive and noble gas species including helium-4 (^4He). Noble gases analyzed with portable mass spectrometry have shed light on various hydrological processes within recent years (e.g., Chatton et al., 2017; Hoffmann et al., 2020; Popp et al., 2020; Schilling et al., 2021; Vautier et al., 2020). Likewise, the noble gas radon-222 (^{222}Rn) is another often used tracer to study surface water-groundwater interactions (e.g., Gleeson et al., 2018). With a half-life of 3.8 days, ^{222}Rn can be used to assess apparent travel times (from here on referred to as travel times or TTs) of up to ~ 15 days of infiltrating river water to groundwater (e.g., Hoehn & Von Gunten, 1989).

However, an accurate interpretation of age dating tracers such as ^{222}Rn activities is inherently challenging because every water sample consists of a mixture of waters with various ages (e.g., Cook & Herczeg, 2000; Jasechko, 2019; Sprenger et al., 2019). Thus, disentangling major flow paths and identifying groundwater mixing processes is key to allow for an accurate interpretation of travel times using age dating tracers (e.g., Sprenger et al., 2019).

The ongoing evolution of mixing models for source partitioning within the hydrological sciences (e.g., Beria et al., 2020; Popp et al., 2019) and beyond (e.g., Stock et al., 2018) provides an often neglected set of toolboxes to account for the various sources of uncertainties related to mixing models. One major limitation of groundwater mixing modeling is to identify end-members correctly and the inability to observe end-members over time (e.g., Carrera et al., 2004; Delsman et al., 2013; McCallum et al., 2010). The assumption of constant end-members cannot be verified or falsified if tracer time-series are unavailable. In fast changing systems though, end-members might in fact be transient. Moreover, a delay between the time a source enters the system and the time it is observed in the mixture is rarely considered (Beria et al., 2020).

In this study, we present a framework with the key objective to determine travel times of a groundwater fraction consisting of recently infiltrated river water (F_{rw}) by first, assessing groundwater mixing between infiltrated river water and regional groundwater using ^4He concentrations combined with a Bayesian end-member mixing model (Popp et al., 2019) and second, inferring transient travel times of F_{rw} employing the mixing adjusted ^{222}Rn activities of F_{rw} . To this end, we continuously analyzed dissolved noble gases (^4He , ^{222}Rn) on-site during a pumping test lasting seven weeks conducted at a wellfield used for the drinking water supply of Bern, Switzerland. The obtained data set is unique in that it provides high-resolution time-series of noble gas concentrations for an end-member and the water mixture. Finally, to test our assumptions as well as to validate the tracer-based results, we compared groundwater mixing ratios obtained from the noble gas analysis with those derived from a fully coupled and calibrated numerical surface water-groundwater model of the wellfield built in *HydroGeoSphere* (HGS; Aquanty Inc., 2015).

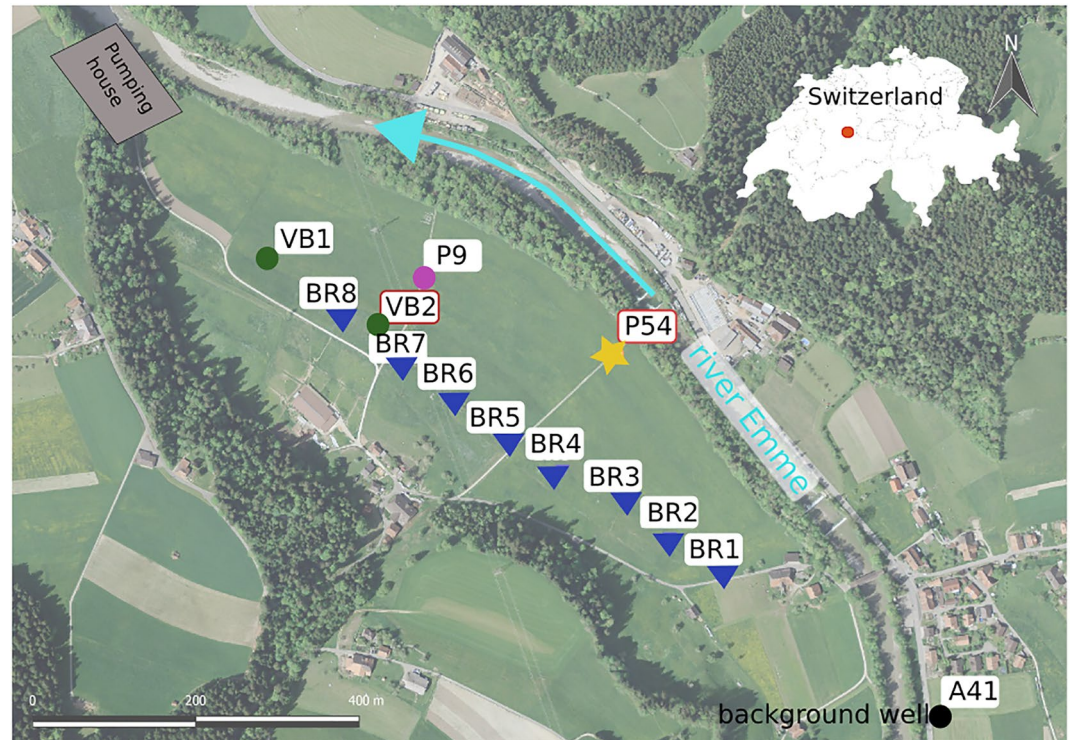


Figure 1. Study area showing the pumping well gallery (BR1–BR8 in blue), two newly installed pumping wells (VB1 and VB2 in green), the location of the pumping house as well as the piezometers P54 (orange), P9 (magenta), and A41 (black). The red dot on the Swiss map indicates the location of the study site.

2. Materials and Methods

2.1. Site Description

This study was conducted in the alluvial catchment of the river Emme, located at the northern margin of the Swiss Alps (Figure 1). We focus on the lower part of the catchment, which consists of the river Emme and the underlying alluvial aquifer. The river exhibits a coarse gravel and sand riverbed with a very dynamic discharge, which is usually highest during snowmelt from April to May (Käser & Hunkeler, 2015).

The alluvial aquifer has an average thickness of about 25 m and can extend up to 46 m. At our study location, the valley is between 200 and 400 m wide (Würsten, 1991). The upper part of the aquifer is predominantly unconfined, and is filled with coarse sandy gravel and cobbles with variable fractions of silt. The saturated hydraulic conductivity of the alluvial aquifer is relatively high (~ 500 m/d), compared to the estimated mean hydraulic conductivity of the river bed (~ 2.5 m/d) (Schilling et al., 2017). The lower part of the alluvium overlying the bedrock consists of up to 3 m thick silty material, which hydraulically disconnects the bedrock from the alluvial aquifer (Blau & Muchenberger, 1997).

A wellfield consisting of eight wells (BR1–BR8), aligned in parallel to the river Emme abstracts on average a total of 24,000 L/min of groundwater (Figure 1). Wells BR1 to BR3 pump water from 10 m depth, whereas wells BR4 to BR8 withdraw water from 15 m depth (Käser & Hunkeler, 2015).

Water source partitioning as well as groundwater travel times at this study site are particularly important in the context of current and projected environmental changes. Michel et al. (2020), for example, found that between 1999 and 2018 the annual discharge of the Emme already decreased each decade by $12\% \pm 4\%$. Additionally, Addor et al. (2014) showed that river discharge in the Emmental catchment is projected to further decrease by 25%–45% in summer (for the years 2070–2099) in response to increasing air temperatures. Changes in river discharge naturally also alter groundwater recharge patterns and are likely to impact water

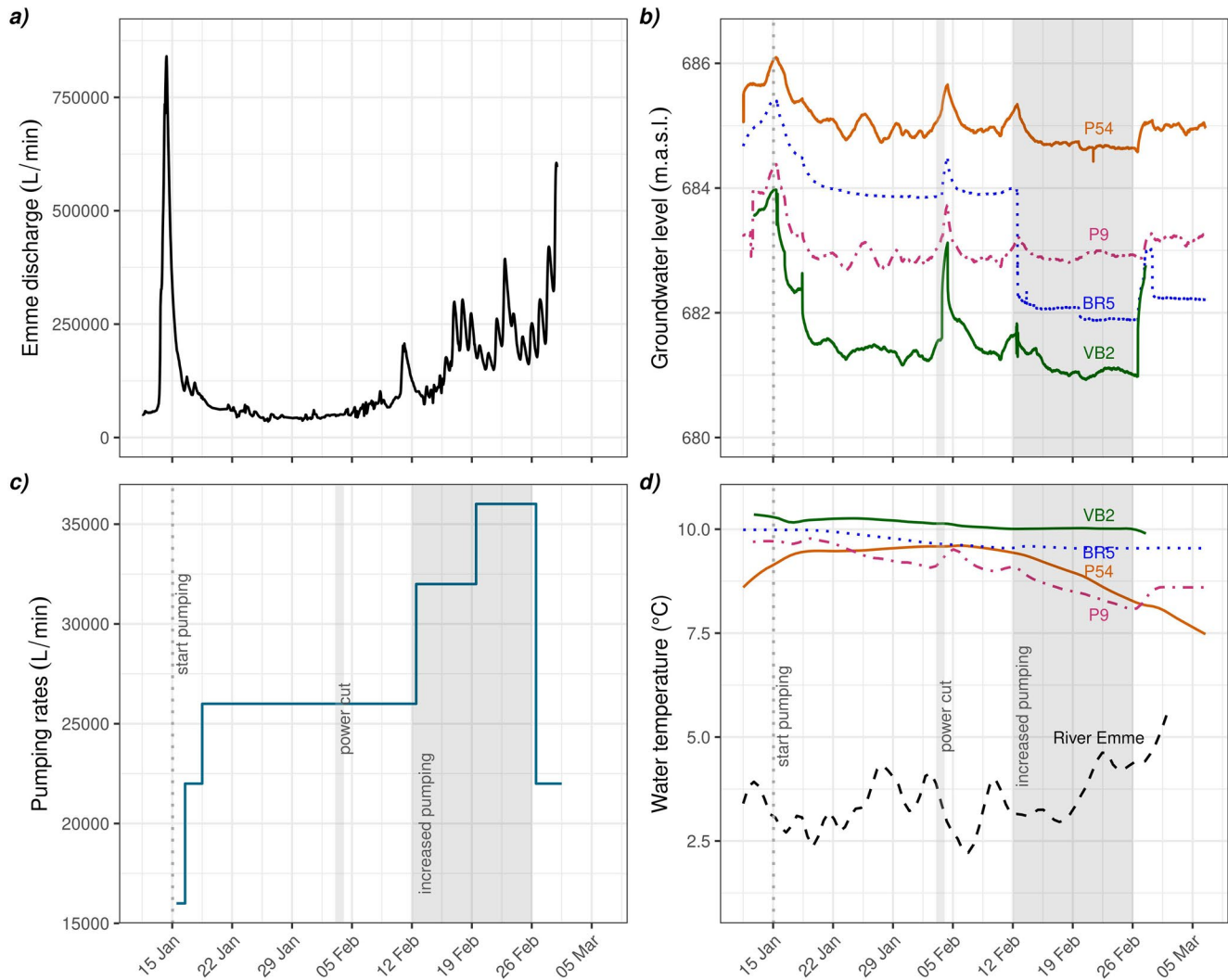


Figure 2. Prevailing conditions during the experiment: (a) the discharge of the Emme (recorded at Heidebühl-Eggwil ~8 km upstream of the study site), (b) groundwater levels of P54 (orange), VB2 (green), BR5 (dotted, blue) and P9 (dashed, magenta), (c) the total sum of groundwater pumped and (d) water temperatures of P54, VB2, BR5, P9 and the river Emme (dashed, black). The dark gray segment indicates the period of increased pumping (February 12–26). Light gray bands indicate an electric power cut occurring at the study site, which caused a shutdown of all wells from February 3, 6:30 p.m., to the following morning at 10 a.m.

quality (Hock et al., 2019). Consequently, anticipated environmental changes are expected to negatively affect the drinking water production of the study area.

2.2. Controlled Forcing of the System Through a Pumping Test

From January 15 to February 26, 2019, a pumping test was conducted, primarily using two newly installed wells (VB1 = 41 m deep and VB2 = 26 m deep, screened from 6 m depth to the bottom of the borehole) as well as already existing wells (BR4–BR8; Figure 1).

Figure 2a and 2b show the dynamics of the prevailing hydraulic conditions during the pumping test, and Figure 2d shows the water temperatures. Figure 2c depicts the three main phases of the pumping test: (1) January 15 marks the beginning of the pumping test when pumping started with 16,000 L/min equally withdrawn from VB1 and VB2, and was gradually increased to 26,000 L/min (14,000 L/min from VB1 and 12,000 L/min from VB2) until January 18; (2) from February 12 to 26, pumping was further increased to reach an overall maximum pumping rate of 36,000 L/min by employing BR4 to BR8 (11,000 L/min) in

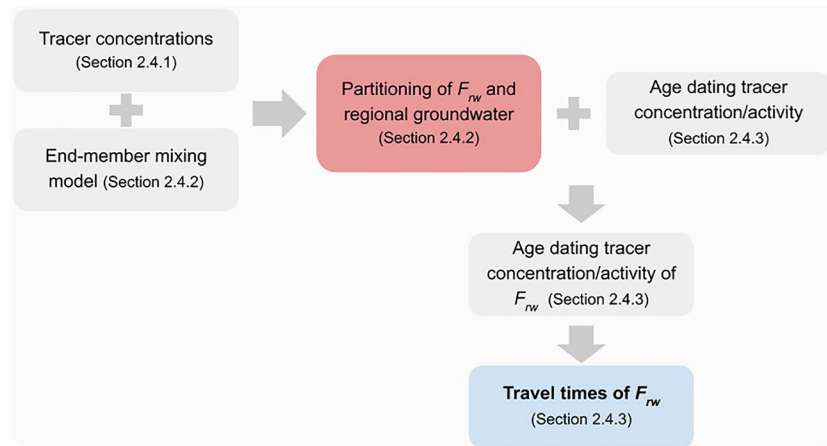


Figure 3. Framework illustrating the approach of determining travel times of a water fraction based on the previous estimation of mixing ratios using a combination of tracer data and end-member mixing modeling.

addition to VB1 (14,000 L/min) and VB2 (11,000 L/min); (3) on February 26, the pumping test was completed and the pumping regime at the drinking water production site went back to normal operating conditions (i.e., using BR1–BR8 only). Please note that there was a complete shutdown of all pumps from January 10 to 15. All pumping rate data can be found in Table S1 (Supporting Information).

2.3. Methodological Framework

Figure 3 illustrates the framework introduced by this study. The aim is to first partition the major groundwater sources (red box) to ultimately infer the travel times of the recently infiltrated water fraction (F_{rw} ; blue box). The following sections explain the used tracer data and modeling approaches.

2.4. Tracer-Based Approach

2.4.1. Theory and Dissolved (Noble) Gas Analyses

The activities of the radioactive noble gas ^{222}Rn increase non-linearly in groundwater and eventually reach a secular equilibrium after ~ 20 days (~ 5 half-lives; Krishnaswami et al., 1982). The Earth's atmosphere has virtually no source of ^{222}Rn , therefore, water in equilibrium with the atmosphere is practically devoid of radon (e.g., Cook & Herczeg, 2000; Figure 4). The absence of ^{222}Rn in air-equilibrated water and its

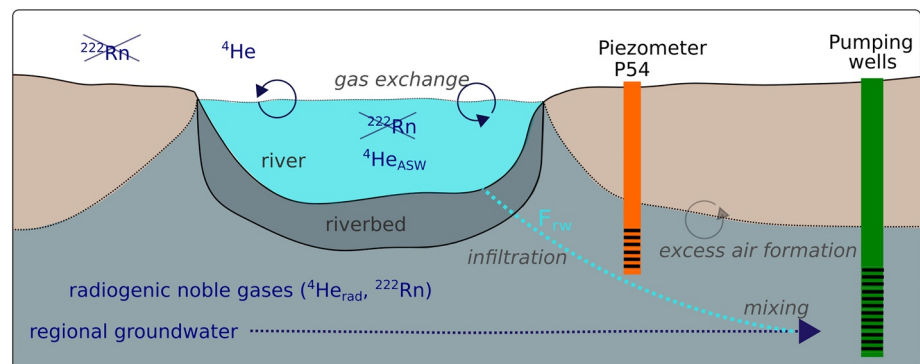


Figure 4. Conceptual model of processes (in *italic*) affecting the noble gas composition of groundwater at a losing stream reach: the ^4He concentration of the river is solely affected by gas exchange with the atmosphere; once the river infiltrates, ^4He is added due to excess air formation. The admixture of $^4\text{He}_{\text{rad}}$ -enriched older groundwater causes a further increase in ^4He concentrations. ^{222}Rn starts to accumulate once river water infiltrates. Please note that the groundwater flow paths are mostly parallel to the river (see Figure S4, SI).

short half-life render ^{222}Rn an excellent tracer to study surface water-groundwater interactions (e.g., Bourke et al., 2014; Gleeson et al., 2018; Hoehn et al., 1992).

Different to ^{222}Rn , ^4He is a stable noble gas (isotope), which is either of atmospheric or radiogenic origin (Figure 4). The concentration of ^4He dissolved in groundwater ($^4\text{He}_{\text{gw}}$) is given by

$$^4\text{He}_{\text{gw}} = ^4\text{He}_{\text{asw}} + ^4\text{He}_{\text{ea}} + ^4\text{He}_{\text{rad}} \quad (1)$$

where $^4\text{He}_{\text{asw}}$ corresponds to the helium in air-saturated water (ASW) at a given water temperature, pressure and salinity, $^4\text{He}_{\text{ea}}$ is helium originating from excess air formation (i.e., the partial dissolution of air entrapment at recharge and water table fluctuations; Heaton & Vogel, 1981) and $^4\text{He}_{\text{rad}}$ represents radiogenic helium accumulated underground (e.g., Cook & Herczeg, 2000).

Recently infiltrated river water presumably does not contain any $^4\text{He}_{\text{rad}}$ (Gardner et al., 2011). Thus, any excess in $^4\text{He}_{\text{gw}}$ (relative to atmospheric-derived ^4He , i.e., $^4\text{He}_{\text{asw}}$ and $^4\text{He}_{\text{ea}}$) indicates an admixture of older groundwater containing $^4\text{He}_{\text{rad}}$ due to longer travel times (Figure 4). In this study, we assume (i) that the observed dynamics of helium concentrations are governed by changes in excess air formation in end-member 1 (i.e., recently recharged water from the river), (ii) that the helium in end-member 2 (i.e., the regional groundwater) remains constant within the studied wellfield, and (iii) that no additional excess air is formed after the point in time when the end-members were analyzed in the piezometers P54 and A41, respectively. We consequently use the total helium concentration differences between the two end-members for the end-member mixing model, as it is done with any other conservative tracer.

The dissolved (noble) gases were analyzed at two locations: in Piezometer P54 and in the pumping house (Figure 1). P54 serves as a proxy for infiltrated river water due to its close proximity to the Emme (~50 m). There, a submersible pump (Comet ECO-PLUS_20000) abstracted ~3 L/min from a depth of 6 m (well depth is 8 m with 2 m screen at the bottom). In the pumping house, we first only analyzed water originating from the newly installed pumping well VB2. VB2 is located in about 220 m distance to the river. Water from VB2 was abstracted by two submersible pumps (8 and 10 m below ground) and parts of it were diverted to the pumping house. The remaining part of the water abstracted at VB2 and all water pumped at VB1 were discharged to the river, thus, the water pumped from VB1 (by two submersible pumps, 8 and 10 m below ground) was at no point of this experiment contributing to the water mixture analyzed in the pumping house. To increase the pumping rate, the existing Wells BR4-8 were turned on progressively on February 12 (Table S1) and all the pumped water mixture went to the pumping house. At the same time, all water from VB2 was discharged into the river. This means that from February 12 on, the water being analyzed in the pumping house was a water mixture originating from the wellfield (i.e., BR4-8; Table S1). At both locations (i.e., inside the pumping house and inside a wooden hut at P54; Figure S1), we continuously analyzed dissolved ^{222}Rn using a Rad7 instrument (DURRIDGE, 2019) as well as ^4He employing the GE-MIMS system. The two instruments were operated in parallel by allocating ~1.5 L/min of pumped water to each instrument. Sampling resolution of the Rad7 was 30 min per sample and ~10 min per sample for the GE-MIMS. For air-water equilibration, we used commercially available membrane modules (3M Liqui-Cel, 2017) for all instruments. Gas sampling and analysis were conducted in exactly the same way at both locations. More details on continuous noble gas analyses are available in Text S1.

2.4.2. Tracer-Based Mixing Ratios

As previously shown (e.g., Carrera et al., 2004; Delsman et al., 2013; Hooper, 2003; Popp et al., 2019), estimated water mixing ratios based on tracer-aided end-member mixing models can exhibit large uncertainties. Uncertainties can originate, for instance, from using tracers that are not truly conservative (e.g., Valder et al., 2012), by not identifying all end-members correctly (Carrera et al., 2004; Delsman et al., 2013) and because end-members (and their associated tracer signals) are not constant in time (e.g., Hooper et al., 1990). These uncertainties are still often neglected, preventing a meaningful analysis of model errors, which can in turn lead to an erroneous interpretation of the results.

To quantify and account for these uncertainties, we applied a Bayesian groundwater mixing approach (see Popp et al., 2019) using hourly aggregated ^4He concentrations as tracers. This approach allows to explicitly account for sampling and measurement uncertainties (Popp et al., 2019). The model in this study was

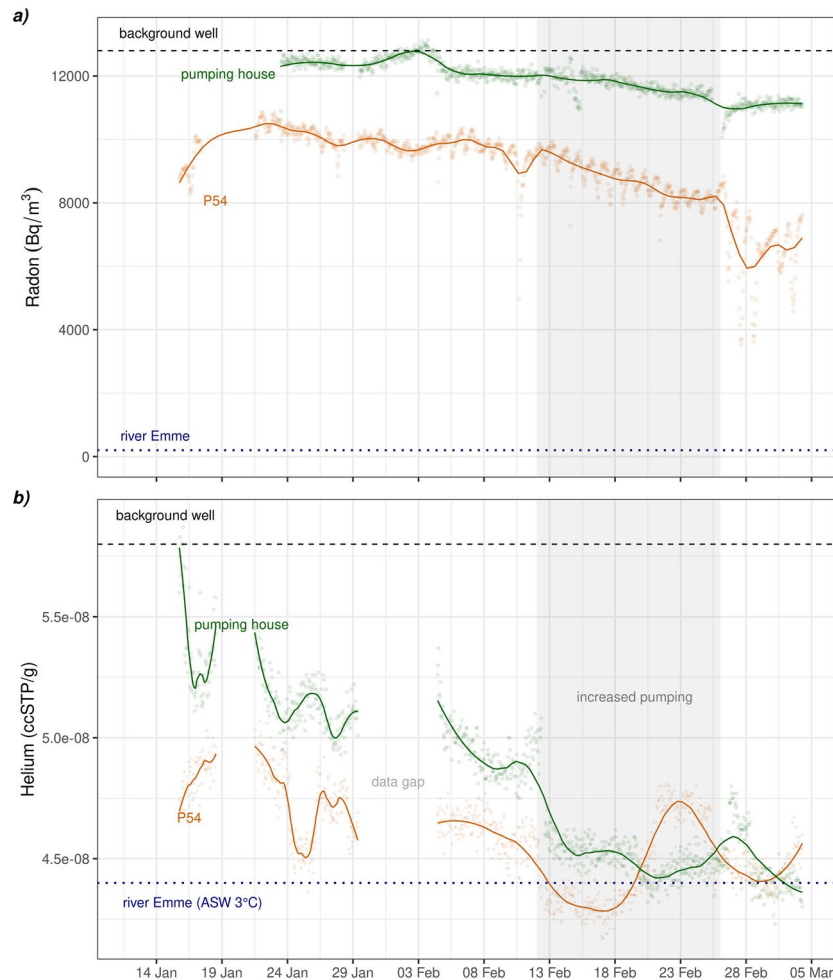


Figure 5. (a) ^{222}Rn activities and (b) ^4He concentrations continuously analyzed at P54 (orange) and in the pumping house (green); the background well (A41, black dashed line) represents regional groundwater; ASW (blue dotted line) represents the average ^4He concentration of the river water. Gray segments indicate the period of increased pumping. Note that no error bars are shown because the analytical uncertainty of both tracer methods is lower than the temporal variability seen in the data points.

simplified by excluding the possibility of unknown end-members based on a sound conceptual understanding of the area from previous studies (Käser & Hunkeler, 2015; Schilling et al., 2017; Tang et al., 2018). Accordingly, we defined two end-members. For the end-member mixing modeling approach, end-member 1 (E_1) is represented by P54, given its proximity to the river. We thereby assume that E_1 consists entirely of recently infiltrated river water, containing excess air but no $^4\text{He}_{\text{rad}}$ —an assumption that was supported by the numerical model (see Section 3.2). End-member 2 (E_2) is represented by piezometer A41 (~ 20 m deep; Figure 1), that previously served as background piezometer for regional groundwater by Schilling et al. (2017). There are no high-resolution tracer data available for the background well. However, following Schilling et al. (2017), time-series data seem dispensable since this piezometer was identified to hardly be affected by seasonal changes or groundwater pumping. The ^4He concentration of end-member E_2 is thus assumed to be constant over time, which is why there is no time dependency given for E_2 in Equation 2. The measured ^4He concentrations at E_1 , however, are dynamic (Figure 5). Consequently, we assume, similar to Brewer et al. (2002), that for every point in time t the following relationship holds for the water mixture $C_{\text{mix}}(t)$ observed in the pumping house:

$$C_{\text{mix}}(t) = F_{\text{rw}}(t)\tilde{C}_{E_1}(t) + F_{\text{ogw}}(t)C_{E_2} \quad (2)$$

where F_{rw} is the fraction of recently infiltrated river water, F_{ogw} the fraction of older, regional groundwater, C_{E_2} is the concentration of a tracer observed at end-member E_2 and $\tilde{C}_{E_1}(t)$ is a *time averaged* concentration observed at the dynamic end-member E_1 . Equation 2 is solved for F_{rw} , while F_{ogw} is per definition $1 - F_{rw}$.

Since the transit time between end-member 1 and the wellfield is unknown, we tested the sensitivity of estimated mixing ratios to potential delays, that is, the time the water/tracer needs to travel from P54 to the wellfield. To this end, we imposed different time lags (1–10 days) with one day increments on the tracer used for the mixing model, where the tracer time series was shifted for a particular time lag and the mixing ratios were calculated for the according tracer concentrations shifted in time. The 10 days represent the upper end of the possible time lag—an assumption based on artificial tracer tests (using uranine and naphthionat), which were conducted as part of the pumping experiment. The artificial tracer tests suggest groundwater flow rates between 45 and 100 m/d within the study domain. To represent the delay in flow time and dispersion, the mixing ratios are calculated with the averaged concentration

$$\tilde{C}_{E_1}(t) = \int_0^{\infty} w(\tau) C_{E_1}(t - \tau) d\tau \quad (3)$$

where $w(\tau)$ is the density function of a gamma distribution with a mean μ_{delay} and a relative standard deviation σ_{delay} , defined as 15% of μ_{delay} . We choose a gamma distribution, however, a different parametric family, for instance an inverse Gaussian distribution, would lead to the same results as long as the mode is far from zero (which is the case for how we defined the distribution). Therefore, the choice of the parametric family is negligible if the shape parameter is larger than one. As prior we used a uniform Dirichlet distribution with $\alpha = 1$.

The only constraints of our mixing modeling approach are that the mixing ratios are positive and sum up to one. Mixing ratios are estimated for every point in time independently. Deviations from Equation 2 are assumed to stem only from observational errors due to tracer-related uncertainties. These errors were modeled as normal distributions with relative standard deviations.

Employing the Bayesian mixing model, we assumed an overall uncertainty of 5% for E_1 and for each individual measurement of the analyzed water mixtures. These uncertainties are based on analytical errors ($\sim 2\%$) plus $\sim 3\%$ due to inconsistencies in sampling and analytical procedures. For E_2 , we allocated an overall uncertainty of 10% due to the strong assumptions of having steady-state conditions at this location and that A41 truly represents regional groundwater (similar to Popp et al., 2019). The aforementioned uncertainties also acknowledge the possibility of other water sources (such as snowmelt) contributing to the water mixture, which we assume to have a negligible impact on the tracer concentrations.

This approach consequently allowed us to estimate the recently infiltrated river water fraction of the groundwater mixtures analyzed in the pumping house.

2.4.3. Estimating Travel Times of F_{rw}

Having estimated F_{rw} , we were able to determine the radon activities originating from this water fraction ($Rn_{F_{rw}}$) assuming that ^{222}Rn activities of E_2 (Rn_{E_2}) equal those of the background well. We assume that the water in the background well exhibits steady-state ^{222}Rn activities due to its long residence time (Schilling et al., 2017):

$$Rn_{F_{rw}}(t) = \frac{(Rn_{\text{mix}}(t) - (1 - F_{rw}(t))Rn_{E_2})}{F_{rw}(t)} \quad (4)$$

where $Rn_{(\text{mix})}$ is the ^{222}Rn activity of the water mixture analyzed in the pumping house.

Consequently, we estimated travel times in days (d) using hourly aggregated ^{222}Rn activities (number of observations, $n = 911$) analyzed in the pumping house by means of the ^{222}Rn in-growth approach (Hoehn & Von Gunten, 1989; see Figure S2 for the in-growth curve):

$$TT(t) = \lambda^{-1} * \ln \frac{(Rn_{E_2} - Rn_{river})}{(Rn_{E_2} - Rn_{F_{rw}(t)})} \quad (5)$$

where λ is the radioactive decay constant (0.183 day^{-1} ; Hoehn & Von Gunten, 1989) and Rn_{river} corresponds to the mean radon activity analyzed in the river Emme. Please note that the ^{222}Rn activities of P54 are not included in the calculation of the travel times. While the water of P54 represents an end-member for the ^4He concentrations, it is not an end-member for ^{222}Rn due to its short half-life.

2.5. Simulation-Based Approach

To compare and validate tracer-based mixing ratios with those from a calibrated numerical model (from here on referred to as simulation-based mixing ratios), we used a model built in HGS combined with the *Hydraulic Mixing-Cell* flow tracking tool (HMC; Partington et al., 2011) to determine water mixing throughout the model domain.

HGS is able to simulate both surface water and groundwater flow in a fully integrated way, that means, precipitation partitions into all parts of the water cycle (e.g., groundwater recharge, snow, streamflow, evapotranspiration) in a physically based manner, making it unnecessary to artificially impose these components as boundary conditions. HGS solves a modified version of the Richard's equation using the van Genuchten parametrization. This allows for the simulation of variably saturated subsurface flow, which is particularly important when simulating river-aquifer interactions (Brunner & Simmons, 2012; Schilling et al., 2017). Different to particle tracking, HMC is based on an efficient mixing cell approach (Harrington et al., 1999; Rao & Hathaway, 1989), automatically tracking all water that enters the model domain via specified boundary conditions. HMC thus provides transient mixing ratios of all water sources in every model cell at every time step, and this for marginal extra computational costs (Partington et al., 2011).

We adopted the existing model built and calibrated by Schilling et al. (2017), thus our model setup equals the description therein. Before the transient simulation of the pumping experiment, a quasi-steady-state simulation with constant forcing for 2,586 days (corresponding to the forcing observed at the beginning of the transient simulation period) was carried out, to obtain an equilibrated initial distribution of water sources for subsequent transient HMC analyses. For the transient simulations, all boundary conditions (i.e., river discharge, groundwater heads and precipitation) were updated according to corresponding values at the time of our experiment. In contrast to Schilling et al. (2017), we explicitly simulated snow accumulation and snowmelt (Jonas et al., 2009; Magnusson et al., 2014; Schilling, Park, et al., 2019), because winter conditions were prevalent during a significant part of our experiment.

3. Results

3.1. Continuously Analyzed Dissolved (Noble) Gases

Figure 5 shows the ^{222}Rn activities (a) and ^4He concentrations (b) synoptically analyzed at P54 and in the pumping house. The illustrated data were hourly aggregated (single data points) and smoothed to facilitate visualization (data line). For data smoothing, we applied local polynomial regression fitting (i.e., LOESS; Jacoby, 2000) to all data sets shown in Figures 5 and 7 to reduce noise and increase readability.

As expected, ^{222}Rn activities and ^4He concentrations are lower at P54 than the observations made in the pumping house, except for a short period in February. The ^{222}Rn activities observed in the pumping house temporarily reached the secular equilibrium (i.e., $12,500 \pm 1,300 \text{ Bq/m}^3$ observed at A41, $n = 14$). ^{222}Rn activities recorded at P54, however, have not reached the secular equilibrium. The activities obtained at P54 indicate the relative long time the river water needs to pass through the streambed, which has a low hydraulic conductivity compared to the aquifer (Schilling et al., 2017; Tang et al., 2018). ^4He concentrations observed at P54 are closer aligned to the ^4He concentrations of air-saturated water (ASW) at 3°C (reflecting the ^4He concentration of the prevalent mean Emme water temperature) than the background well.

Although both tracers (^4He and ^{222}Rn) exhibit temporal fluctuations, the overall trend shows a decrease in both tracers for the duration of our experiment. Please note that we assumed the tracer activity/concentration

for end-member 2 (i.e., the background well) to be constant over time. Also note that we did not detect any considerable ^{222}Rn activities in the river Emme during sporadic sampling (mean activity $199 \pm 139 \text{ Bq/m}^3$, $n = 13$), which indicates that the river was not gaining any relevant amounts of groundwater during the period of our experiment.

3.2. Tracer-Based and Simulation-Based Estimates of F_{rw}

Figure 6 shows the estimated fraction of recently infiltrated river water for the wellfield (i.e., water mixture analyzed in the pumping house) inferred from the tracer-based (various colors) and the simulation-based approach (dashed, black). Since F_{rw} observed in the pumping house results from a mixture of waters coming from different pumping wells, we calculated the simulated F_{rw} values (derived from the numerical model) as a weighted mean according to the relative water contribution from each well to the water mixture. The dashed black line in Figure 6 thus illustrates a weighted mean of F_{rw} equivalent to the groundwater mixture analyzed in the pumping house.

Figure 5 highlights that the assumption of time-invariant end-members does not hold for our data because the tracer concentrations observed at P54 vary within the observation period. However, Figure 6 shows no distinct differences in mixing ratios when imposing different time delays (i.e., 1–10 days), suggesting that the influence of a potential time lag on the estimated mixing ratios is negligible. Consequently, all data regarding F_{rw} correspond from here on to the estimated mixing ratios with no imposed time lag (pink data shown in Figure 6).

Generally, the tracer-based and simulation-based mixing ratios agree reasonably well within the calculated uncertainties, except for the beginning of the experiment. For the entire duration of the experiment, the tracer-based and simulation-based estimates predict an average of $67\% \pm 23\%$ and $70\% \pm 4\%$ of water originating from recently infiltrated river water, respectively. The experiment can be divided in three major phases: before, during and after the pumping was increased (Table 1 and Figure 2c). The tracer-based calculations show an increase from about $57\% \pm 25\%$ (period before the pumping increased) to a mean value of $75\% \pm 21\%$ for the time of increased pumping. After the pumping regime went back to normal operation conditions, F_{rw} first slightly dropped but then increased again. The simulated estimates of F_{rw} show a different trend: after pumping increased, estimates slightly decreased from $74\% \pm 7\%$ to $67\% \pm 3\%$. In the last phase, simulated estimates of F_{rw} slightly increased again to $73\% \pm 3\%$. Although these differences fall in the range of the estimated uncertainties, the trends of the tracer-based and simulation-based mixing ratios do not necessarily correlate (see Discussion for model limitations).

Mixing ratios simulated at P54 confirm that its water consists almost exclusively ($\sim 90\%$) of infiltrated river water. Thus, the assumption to use ^4He concentrations of P54 to characterize the ^4He concentrations of F_{rw} for the groundwater mixing model seems justified.

3.3. Travel Times of F_{rw}

Knowing the fraction of river water within the pumped groundwater, we can use the ^{222}Rn activities of F_{rw} to infer the travel times of F_{rw} to the wellfield. In accordance with the decreasing ^{222}Rn activities observed at P54 and the pumping house (Figures 5 and 7), the estimated TTs show the same decreasing trend over time. On average, the travel time from the river to the wellfield is in the range of 12 ± 3 days. With 14 ± 4 days, the period before the pumping was increased showed the highest mean travel time (Table 1). After pumping was increased, TTs generally decrease until the end of the experiment. Toward the end of February, we obtained travel times as low as 7 ± 2 days.

From the ^{222}Rn activities shown in Figure 5a, it becomes apparent that the recently recharged river water (observed in P54) has already accumulated a substantial amount of the total ^{222}Rn measured in the pumping house, which indicates that a large portion of the total travel time occurs between the stream and P54. Consequently, the travel time between P54 and the wellfield is comparatively fast. This phenomenon can be explained by the lower hydraulic conductivity of the riverbed that the infiltrating river water needs to pass first. For the remaining distance between P54 and the wellfield ($\sim 200\text{--}300$ m), the recently recharged

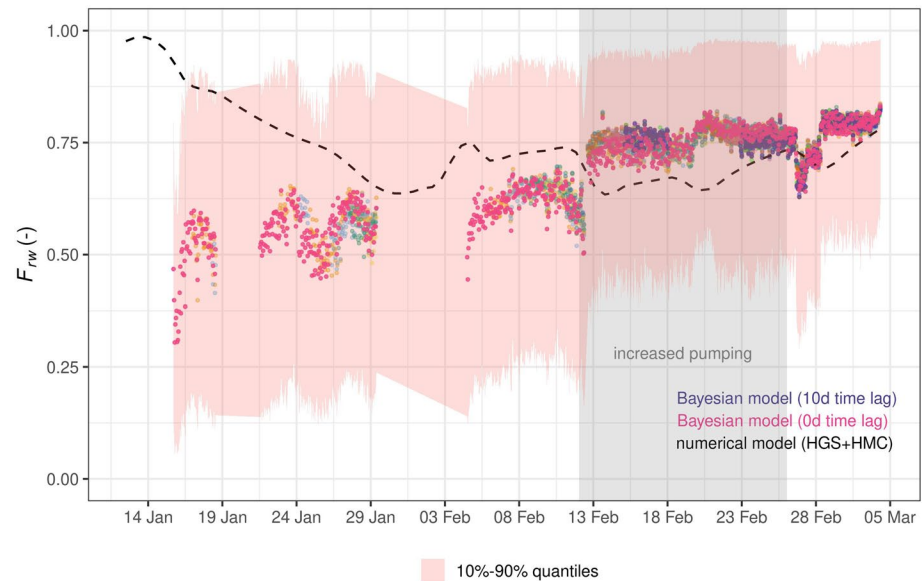


Figure 6. Estimates of F_{rw} (for the water mixture analyzed in the pumping house) from the numerical model (dashed, black line) and from the tracer-based Bayesian model with no time lag (pink), a 10 days time lag (dark-blue) and 1–9 days time lag scenarios (various colors). Error bars indicate the 10% and 90% quantiles derived from the Bayesian model (no time lag).

river water only takes a few days, which aligns well with the results of the artificial tracer test suggesting groundwater flow rates of up to 100 m/d within the aquifer.

Finally, the average travel time (12 ± 3 days; Table 1) using the mixing-corrected ^{222}Rn activities aligns well with the travel time obtained through the artificial tracer test, which revealed a travel time from the injection well (i.e., A41) to VB2 of \sim seven days (Figure S3). Since the tracer was directly injected into the groundwater, the travel time between the point of injection and VB2 is expected to be lower than the TT of F_{rw} because the river water has to pass the low hydraulic conductivity zone of the riverbed before entering the aquifer.

4. Discussion

4.1. Validation of Tracer-Based and Simulation-Based Mixing Ratios

The estimated mixing ratios of the tracer-based and simulation-based approaches agree acceptably well, considering the underlying assumptions and associated uncertainties of both approaches (Figure 6). At the beginning of the pumping test, however, the simulated and tracer-based mixing ratios show considerable dissimilarities.

There are also contrasting effects between the two approaches during the three different phases of the pumping test (Table 1): the simulations generally show lower estimates of F_{rw} during the increased pumping period, whereas the tracer-based estimates of F_{rw} increase steadily from the first to the third phase. These differences most likely reflect the heterogeneity (e.g., causing preferential flow paths) of the aquifer, which the numerical model does not adequately reproduce because the aquifer and the streambed are both represented by homogeneous hydraulic conductivities.

Besides comparing tracer-based and simulation-based mixing ratios, we can also compare our tracer-based results with results of Schilling et al. (2017). Using a combination of different tracers including ^{222}Rn , ^{37}Ar , $^3\text{H}/^3\text{He}$, and noble gas recharge temperatures, Schilling et al. (2017)

Table 1
Estimates of F_{rw} as Well as Travel Times During the Three Major Phases of the Pumping Test

	Increased pumping		
	Before	During	After
Tracer-based F_{rw} (%)	57 ± 25	75 ± 21	76 ± 20
Simulated F_{rw} (%)	74 ± 7	67 ± 3	73 ± 3
TT (d)	14 ± 4	12 ± 3	9 ± 2

Note. Uncertainty of the simulated F_{rw} refers to the standard deviation of the simulated mean over the respective period.

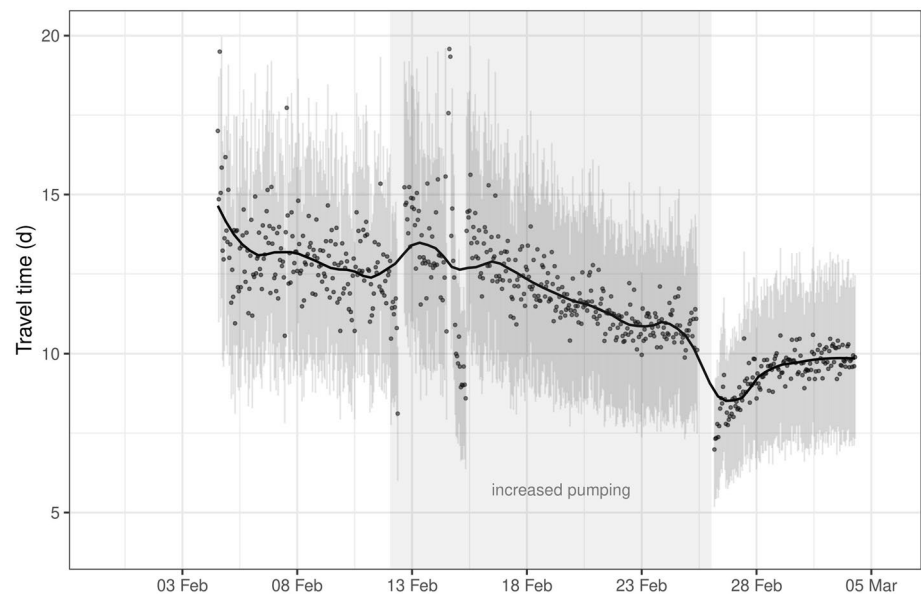


Figure 7. Estimated TTs of F_{rw} for the water mixture analyzed in the pumping house. Error bars indicate propagated uncertainty derived from the Bayesian mixing model (no time lag) and analytical uncertainties.

observed fractions of recently infiltrated river water within a similar range (between 70%–80%) at BR7. Consequently, our estimates of F_{rw} are agree reasonably well with previous results.

The cause for the rise in ^4He concentrations observed in P54 from February 19 to February 23 remains unclear and is not possible to explain without another conservative tracer available. The lack of such is a major shortcoming of this study. We intended to use electrical conductivity as additional conservative tracer, however, the probe we installed in piezometer P54 was not working properly and thus yielded no usable data. Also, the water temperature measurements (Figure 2d) do not provide any additional insight on this matter.

4.2. Impact of Controlled Forcing on Groundwater Levels, Mixing Ratios, and Travel Times

Figure 2b and 2c show that groundwater pumping clearly has an effect on groundwater levels and a minor effect on water temperatures. During the increased pumping phase the tracer-based estimates show an increase in F_{rw} of about 18%, while the estimated travel times decrease about 14% in comparison to the previous phase (Table 1). These changes are most likely related to the change in the pumping regime once pumping was increased because the analyzed water originated no longer from VB2 but from a mixture of waters from different wells that are about 10 m less deep than VB2. We hypothesize that the elevated well depths, in turn, most likely influence F_{rw} .

From previous (e.g., Schilling et al., 2017; Tang et al., 2018) and our own results, we conclude that groundwater flow paths and travel times exhibit a temporal variability, which are only to some extent governed by the applied groundwater pumping rates. We explain this relatively low sensitivity against hydraulic forcing by the high hydraulic conductivity of an aquifer with a large transmissivity and thus high storage capacity: the high hydraulic conductivity enables large amounts of river water to infiltrate at various locations upstream of the catchment. An infiltration spread over a large area results in an overall large F_{rw} in the groundwater mixture, regardless of the intensity of the applied groundwater pumping. Another factor is the high hydraulic gradient (Figure 2b), which induces a high groundwater flux relative to pumping. Moreover, temporal trends of F_{rw} (e.g., increase in F_{rw} and decrease in travel times) also seem partially controlled by the rise in river discharge (thereby enhancing infiltration rates) over the duration of this experiment (Figure 2a). This assumption is also supported by the increase in mixing ratios (Figure 6) within the last days of the experiment (after pumping was shut-down), which can only be explained by an increased river discharge (Figure 2a) and not by any pumping-related activities. Consequently, river discharge appears to have a large control of mixing between river water and groundwater in the studied aquifer. We would like to

highlight though that the mixing ratios and travel times are governed by several processes (i.e., the changes in pumping rates and pumping wells and their depths as well as the river discharge). The methods we used here do not allow us to disentangle the different effects, which is, however, also beyond the purpose of this study.

4.3. Limitations of Estimated F_{rw} and Travel Times

Despite the acceptable agreement of estimated mixing ratios by two independently executed methods, this study has several limitations. Since any water sample is a mixture of waters with a distribution of travel times, any interpretation of tracer data is challenging and potentially erroneous (e.g., Jasechko, 2019; Sprenger et al., 2019). Ideally, we would have analyzed multiple age-dating tracers (e.g., ^{37}Ar , ^{35}S , and $^3\text{H}/^3\text{He}$) to capture a wider range of potential water ages. However, such tracer studies cannot be carried out at a high spatial and temporal resolution since they are typically costly and unfeasible to sample with a high temporal resolution. Also, only specialized laboratories are able to conduct such analyses. Additionally, it would have been very helpful to better constrain the mixing ratios by using a combination of conservative tracers because the tracer set size and composition can influence the estimated mixing ratios (Barthold et al., 2011; Popp et al., 2019).

We are also aware that not everyone has two portable GE-MIMS systems and two Rad7 instruments available. Another potential way of using the introduced framework would be a combination of high-resolution sampling of other, cheaper conservative tracers (e.g., electrical conductivity) and grab sampling of specialized tracers (e.g., noble gases such as ^4He or ^{37}Ar).

Moreover, we acknowledge that the possible dating range of ^{222}Rn might not capture the actual distribution of travel times of F_{rw} . As indicated by the results of this study (Figure 7) and Schilling et al. (2017), travel times temporarily exceed the reliable dating range of ^{222}Rn (i.e., 0–15 days). However, we argue that in the context of drinking water production from bank filtrate, the identification of water fractions younger than two weeks is most relevant. This is particularly true for Switzerland where, according to the water protection law (GSchV, SR 814.201), groundwater used for drinking water production must have a travel time of at least 10 days within the relevant protection zone. Thus, in terms of drinking water supply, a conservative estimate of the lower limit of travel times of recently infiltrated surface water is of the highest interest.

Lastly, we would like to acknowledge the assumption that the infiltration signal at P54 is representative of the entire reach, although the infiltrated river water observed at P54 only integrates a small fraction of the aquifer. By using the tracer signal of P54 we assume that no natural variability of the river bed and bank exists (e.g., variable riverbed thickness or hydraulic conductivity), which could potentially influence stream water infiltration pattern.

5. Conclusions and Implications

The primary goal of this study was to develop a framework (Figure 3) that enables a meaningful interpretation of a water age dating tracer by first partitioning major water sources and second interpreting the age dating tracer concentration/activity of the water fraction of interest. We applied this approach using a combination of in-situ analyzed tracer data and modeling under partially controlled forcing conditions (i.e., a groundwater pumping test). In summary, the study provides the following methodological advancements for tracer hydrology:

- Partitioning major water sources enables the interpretation of an age dating tracer (here ^{222}Rn activities) of the recently infiltrated water fraction (Figure 7)
- We explicitly account for all uncertainties related to model assumptions and tracer measurements by employing a Bayesian mixing model. This approach enables us to quantify model uncertainties, propagate these uncertainties to the estimated travel times and generally allows us to test assumptions posteriori (Figure 6)
- We demonstrate the continuous, on-site use of state-of-the-art tracer techniques to elucidate the transience of water sources and mixtures (Figure 5). Without high-resolution time-series data, the system

response to forcing (either in the form of groundwater pumping or increased river discharge) cannot be assessed properly

- Furthermore, the continuous observation of an end-member demonstrates that the common assumption of constant end-members can be inaccurate. At the same time, testing the sensitivity of the estimated mixing ratios to different imposed time lags (i.e., the delay between the time a source/end-member enters the system and the time it is observed in the mixture) showed that a time lag seems to have negligible influence on the estimated mixing ratios, at least for the studied wellfield and the available data set
- Although applied here with two specific tracers, the framework can be used with other suitable tracers (dependent on the system of interest)

Additionally, our results imply the following insights for an improved system understanding of an alluvial, pre-alpine aquifer and water resources management:

- On average, a substantial fraction (~70%) of abstracted groundwater originates from recently infiltrated river water (Table 1 and Figure 6)
- F_{rw} exhibits travel times in the order of two weeks but can be as low as 7 ± 2 days (Figure 7)
- Our findings (i.e., observed ^{222}Rn activities) indicate that the streambed has a major control on the travel times of infiltrating stream water (Figure 5a) causing relatively long travel times between the stream and the streambank, relative to the total estimated travel times from the stream to the wellfield
- All three previous points are highly relevant for drinking water supply systems at similar sites using bank filtrate

Overall, these findings (particularly the high fraction of F_{rw} in the abstracted groundwater and its short travel times) suggest that the system studied is vulnerable to current and anticipated environmental changes such as increasing contamination and summer droughts.

Data Availability Statement

All data and code used in this study can be found in the Supplementary Information.

Acknowledgments

The authors thank three anonymous reviewers and the associate editor for their constructive comments, which helped to improve this manuscript. The authors thank Laurent Marguet, Roberto Costa, Reto Britt, and Kay Fries for their support in the field. The authors thank the Tracerlabor Dr. Wernli and the Bau- und Verkehrsdirektion des Kantons Bern for providing the artificial tracer test data. Moreover, the authors are grateful for the fieldwork planning support from the Bau- und Verkehrsdirektion des Kantons Bern as well as for the model input data provided by the Federal Office for the Environment (BAFU), MeteoSwiss and the Canton of Bern. Andrea L. Popp and Álvaro Pardo-Álvarez gratefully acknowledge financial support for this work from the EU Framework Programme for Research and Innovation Horizon 2020 ITNs “Hypotrains” (grant no. 641939) and “Enigma” (grant no. 722028), respectively. Andrea L. Popp also acknowledges financial support from Eawag. Oliver S. Schilling and Morgan Peel gratefully acknowledge the funding provided by the Swiss National Science Foundation (grant no. P2NEP2_171985 and 200021_179017, respectively).

References

- Addor, N., Rössler, O., Köplin, N., Huss, M., Weingartner, R., & Seibert, J. (2014). Robust changes and sources of uncertainty in the projected hydrological regimes of Swiss catchments. *Water Resources Research*, 50(10), 7541–7562. <https://doi.org/10.1002/2014WR015549>
- Aquanty Inc. (2015). *HGS reference manual*. Waterloo. Retrieved from <https://static1.squarespace.com/static/54611cc8e4b0f88a2c1abc57/t/59cea33846c3c4384b8e5de1/1506714438873/hydrosphere%5Ctext%5B%5C%5F%5Duser.pdf>
- Barthel, R., & Banzhaf, S. (2016). Groundwater and surface water interaction at the regional scale—A review with focus on regional integrated models. *Water Resources Management*, 30(1), 1–32. <https://doi.org/10.1007/s11269-015-1163-z>
- Barthold, F. K., Tyralla, C., Schneider, K., Vaché, K. B., Frede, H.-G., & Breuer, L. (2011). How many tracers do we need for end member mixing analysis (EMMA)? A sensitivity analysis. *Water Resources Research*, 47(8), 1–14. <https://doi.org/10.1029/2011WR010604>
- Beria, H., Larsen, J. R., Michelon, A., Ceperley, N. C., & Schaeffli, B. (2020). HydroMix v1.0: A new Bayesian mixing framework for attributing uncertain hydrological sources. *Geoscientific Model Development*, 13(5), 2433–2450. <https://doi.org/10.5194/gmd-13-2433-2020>
- Blau, R. V., & Muchenberger, F. (1997). *Grundlagen für Schutz und Bewirtschaftung der Grundwasser des Kantons Bern (Technical Report)*. Bern: Wasser- und Energiewirtschaftsamt des Kantons Bern, Geotechnisches Institut AG.
- Blöschl, G., Hall, J., Viglione, A., Perdigão, R. A. P., Parajka, J., Merz, B., et al. (2019). Changing climate both increases and decreases European river floods. *Nature*, 573(7772), 108–111. <https://doi.org/10.1038/s41586-019-1495-6>
- Boano, F., Harvey, J. W., Marion, A., Packman, A. I., Revelli, R., Ridolfi, L., & Wörman, A. (2014). Hyporheic flow and transport processes: Mechanisms, models, and biogeochemical implications. *Reviews of Geophysics*, 52(4), 603–679. <https://doi.org/10.1002/2012RG000417>
- Bourke, S. A., Cook, P. G., Shanfield, M., Dogramaci, S., & Clark, J. F. (2014). Characterisation of hyporheic exchange in a losing stream using radon-222. *Journal of Hydrology*, 519, 94–105. <https://doi.org/10.1016/j.jhydrol.2014.06.057>
- Brennwald, M. S., Schmidt, M., Oser, J., & Kipfer, R. (2016). A portable and autonomous mass spectrometric system for on-site environmental gas analysis. *Environmental Science & Technology*, 50, 13455. <https://doi.org/10.1021/acs.est.6b03669>
- Brewer, M. J., Soulsby, C., & Dunn, S. M. (2002). A Bayesian model for compositional data analysis. In W. Härdle, & B. Rönz (Eds.), *Comstat* (pp. 105–110). Physica-Verlag HD.
- Brunner, P., & Simmons, C. T. (2012). HydroGeoSphere: A fully integrated, physically based hydrological model. *Ground Water*, 50(2), 170–176. <https://doi.org/10.1111/j.1745-6584.2011.00882.x>
- Brunner, P., Therrien, R., Renard, P., Simmons, C. T., & Franssen, H.-J. H. (2017). Advances in understanding river-groundwater interactions. *Reviews of Geophysics*, 55(3), 818–854. <https://doi.org/10.1002/2017RG000556>
- Carrera, J., Vázquez-Suñé, E., Castillo, O., & Sánchez-Vila, X. (2004). A methodology to compute mixing ratios with uncertain end-members. *Water Resources Research*, 40(12), 1–11. <https://doi.org/10.1029/2003WR002263>
- Chatton, E., Labasque, T., de La Bernardie, J., Guihéneuf, N., Bour, O., & Aquilina, L. (2017). Field continuous measurement of dissolved gases with a cf-mims: Applications to the physics and biogeochemistry of groundwater flow. *Environmental Science & Technology*, 51(2), 846–854. <https://doi.org/10.1021/acs.est.6b03706>

- Cochand, M., Christe, P., Ornstein, P., & Hunkeler, D. (2019). Groundwater storage in high alpine catchments and its contribution to streamflow. *Water Resources Research*, 55(4), 2613–2630. <https://doi.org/10.1029/2018WR022989>
- Cook, P., & Herczeg, A. L. (2000). Environmental tracers in subsurface hydrology (53, No. 9). New York, NY: Springer Science+Business Media. <https://doi.org/10.1017/CBO9781107415324.004>
- Delsman, J. R., Essink, G. H. P. O., Beven, K. J., & Stuyfzand, P. J. (2013). Uncertainty estimation of end-member mixing using generalized likelihood uncertainty estimation (GLUE), applied in a lowland catchment. *Water Resources Research*, 49(8), 4792–4806. <https://doi.org/10.1002/wrcr.20341>
- DURRIDGE. (2019). *Rad7 electronic radon detector—user manual*. Billerica, MA: DURRIDGE Company Inc. Retrieved from <https://www.durridge.com/documentation/RAD7Manual.pdf>
- Fiddes, J., Aalstad, K., & Westermann, S. (2019). Hyper-resolution ensemble-based snow reanalysis in mountain regions using clustering. *Hydrology and Earth System Sciences*, 23(11), 4717–4736. <https://doi.org/10.5194/hess-23-4717-2019>
- Gardner, W. P., Harrington, G. A., Solomon, D. K., & Cook, P. G. (2011). Using terrigenic ⁴He to identify and quantify regional groundwater discharge to streams. *Water Resources Research*, 47(6), 1–13. <https://doi.org/10.1029/2010WR010276>
- Gleeson, T., Manning, A. H., Popp, A., Zane, M., & Clark, J. F. (2018). The suitability of using dissolved gases to determine groundwater discharge to high gradient streams. *Journal of Hydrology*, 557, 561–572. <https://doi.org/10.1016/j.jhydrol.2017.12.022>
- Harrington, G. A., Walker, G. R., Love, A. J., & Narayan, K. A. (1999). A compartmental mixing-cell approach for the quantitative assessment of groundwater dynamics in the Otway Basin, South Australia. *Journal of Hydrology*, 214(1–4), 49–63. [https://doi.org/10.1016/S0022-1694\(98\)00243-1](https://doi.org/10.1016/S0022-1694(98)00243-1)
- Hayashi, M. (2019). Alpine hydrogeology: The critical role of groundwater in sourcing the headwaters of the world. *Groundwater*. <https://doi.org/10.1111/gwat.12965>
- Heaton, T. H. E., & Vogel, J. C. (1981). “Excess air” in groundwater. *Journal of Hydrology*, 50, 201–216. [https://doi.org/10.1016/0022-1694\(81\)90070-6](https://doi.org/10.1016/0022-1694(81)90070-6)
- Herbstritt, B., Gralher, B., & Weiler, M. (2019). Continuous, near-real-time observations of water stable isotope ratios during rainfall and throughfall events. *Hydrology and Earth System Sciences*, 23(7), 3007–3019. <https://doi.org/10.5194/hess-23-3007-2019>
- Hock, R., Rasul, G., Adler, C., Cáceres, B., Gruber, S., Hirabayashi, Y., et al. (2019). Chapter 2: High mountain areas (Tech. Rep.). In H.-O. Pörtner, D. C. Roberts, V. Masson-Delmotte, P. Zhai, M. Tignor, E. Poloczanska, et al. (Eds.), *IPCC special report on the ocean and cryosphere in a changing climate*. NM.
- Hoehn, E., & Von Gunten, H. R. (1989). Radon in groundwater: A tool to assess infiltration from surface waters to aquifers. *Water Resources Research*, 25(8), 1795–1803. <https://doi.org/10.1029/WR025i008p01795>
- Hoehn, E., Von Gunten, H. R., Stauffer, F., & Dracos, T. (1992). Radon-222 as a groundwater tracer. A laboratory study. *Environmental Science & Technology*, 26(4), 734–738. <https://doi.org/10.1021/es00028a010>
- Hoffmann, R., Goderniaux, P., Jamin, P., Chatton, E., de La Bernardie, J., Labasque, T., et al. (2020). Continuous dissolved gas tracing of fracture-matrix exchanges. *Geophysical Research Letters*, 47(17), e2020GL088944. <https://doi.org/10.1029/2020GL088944>
- Holman, I. P. (2006). Climate change impacts on groundwater recharge- uncertainty, shortcomings, and the way forward? *Hydrogeology Journal*, 14(5), 637–647. <https://doi.org/10.1007/s10040-005-0467-0>
- Hooper, R. P. (2003). Diagnostic tools for mixing models of stream water chemistry. *Water Resources Research*, 39(3), 55–61. <https://doi.org/10.1029/2002WR001528>
- Hooper, R. P., Christophersen, N., & Peters, N. E. (1990). Modelling streamwater chemistry as a mixture of soilwater end-members—An application to the Panola Mountain catchment, Georgia, U.S.A. *Journal of Hydrology*, 116(1–4), 321–343. [https://doi.org/10.1016/0022-1694\(90\)90131-G](https://doi.org/10.1016/0022-1694(90)90131-G)
- Huss, M., & Hock, R. (2015). A new model for global glacier change and sea-level rise. *Frontiers of Earth Science*, 3, 1–22. <https://doi.org/10.3389/feart.2015.00054>
- Jacoby, W. G. (2000). Loess: A nonparametric, graphical tool for depicting relationships between variables. *Electoral Studies*, 19(4), 577–613. [https://doi.org/10.1016/S0261-3794\(99\)00028-1](https://doi.org/10.1016/S0261-3794(99)00028-1)
- Jasechko, S. (2019). Global isotope hydrogeology—Review. *Reviews of Geophysics*, 57(3), 835–965. <https://doi.org/10.1029/2018RG000627>
- Jonas, T., Marty, C., & Magnusson, J. (2009). Estimating the snow water equivalent from snow depth measurements in the Swiss Alps. *Journal of Hydrology*, 378(1–2), 161–167. <https://doi.org/10.1016/j.jhydrol.2009.09.021>
- Käser, D., & Hunkeler, D. (2015). Contribution of alluvial groundwater to the outflow of mountainous catchments. *Water Resources Research*, 51, 9127–9140. <https://doi.org/10.1002/2014WR016259>
- Krause, S., Boano, F., Cuthbert, M. O., Fleckenstein, J. H., & Lewandowski, J. (2014). Understanding process dynamics at aquifer-surface water interfaces: An introduction to the special section on new modeling approaches and novel experimental technologies. *Water Resources Research*, 50(2), 1847–1855. <https://doi.org/10.1002/2013WR014755>
- Krishnaswami, S., Graustein, W. C., Turekian, K. K., & Dowd, J. F. (1982). Radium, thorium and radioactive lead isotopes in groundwaters: Application to the in situ determination of adsorption-desorption rate constants and retardation factors. *Water Resources Research*, 18(6), 1663–1675. <https://doi.org/10.1029/WR018i006p01663>
- Lewandowski, J., Arnon, S., Banks, E., Batelaan, O., Betterle, A., Broecker, T., et al. (2019). Is the hyporheic zone relevant beyond the scientific community? *Water*, 11(11), 2230. <https://doi.org/10.1002/2016WR019516>
- Mächler, L., Brennwald, M. S., & Kipfer, R. (2012). Membrane inlet mass spectrometer for the quasi-continuous on-site analysis of dissolved gases in groundwater. *Environmental Science & Technology*, 46(15), 8288–8296. <https://doi.org/10.1021/es3004409>
- Magnusson, J., Gustafsson, D., Hüsler, F., & Jonas, T. (2014). Assimilation of point SWE data into a distributed snow cover model comparing two contrasting methods. *Water Resources Research*, 50(10), 7816–7835. <https://doi.org/10.1002/2014WR015302>
- McCallum, J. L., Cook, P. G., Brunner, P., & Berhane, D. (2010). Solute dynamics during bank storage flows and implications for chemical base flow separation. *Water Resources Research*, 46(7), 1–11. <https://doi.org/10.1029/2009WR008539>
- Michel, A., Brauchli, T., Lehning, M., Schaeffli, B., & Huwald, H. (2020). Stream temperature and discharge evolution in Switzerland over the last 50 years: Annual and seasonal behaviour. *Hydrology and Earth System Sciences*, 24(1), 115–142. <https://doi.org/10.5194/hess-24-115-2020>
- Mutiti, S., & Levy, J. (2010). Using temperature modeling to investigate the temporal variability of riverbed hydraulic conductivity during storm events. *Journal of Hydrology*, 388(3–4), 321–334. <https://doi.org/10.1016/j.jhydrol.2010.05.011>
- Panicorn, C., & Putti, M. (2015). Physically based modeling in catchment hydrology at 50: Survey and outlook. *Water Resources Research*, 51(9), 7090–7129. <https://doi.org/10.1002/2015WR017780>

- Partington, D., Brunner, P., Simmons, C. T., Therrien, R., Werner, A. D., Dandy, G. C., & Maier, H. R. (2011). A hydraulic mixing-cell method to quantify the groundwater component of streamflow within spatially distributed fully integrated surface watergroundwater flow models. *Environmental Modelling & Software*, 26(7), 886–898. <https://doi.org/10.1016/j.envsoft.2011.02.007>
- Partington, D., Therrien, R., Simmons, C. T., & Brunner, P. (2017). Blueprint for a coupled model of sedimentology, hydrology, and hydrogeology in streambeds. *Reviews of Geophysics*, 55(2), 287–309. <https://doi.org/10.1002/2016RG000530>
- Popp, A. L., Manning, C. C., Brennwald, M. S., & Kipfer, R. (2020). A new in situ method for tracing denitrification in riparian groundwater. *Environmental Science & Technology*, 54(3), 1562–1572. <https://doi.org/10.1021/acs.est.9b05393>
- Popp, A. L., Scheidegger, A., Moeck, C., Brennwald, M. S., & Kipfer, R. (2019). Integrating Bayesian groundwater mixing modeling with on-site helium analysis to identify unknown water sources. *Water Resources Research*, 55(12), 10602–10615. <https://doi.org/10.1029/2019WR025677>
- Rao, B. K., & Hathaway, D. L. (1989). A three-dimensional mixing cell solute transport model and its application. *Ground Water*, 27(4), 509–516. <https://doi.org/10.1111/j.1745-6584.1989.tb01971.x>
- Schilling, O. S., Cook, P. G., & Brunner, P. (2019). Beyond classical observations in hydrogeology: The advantages of including exchange flux, temperature, tracer concentration, residence time, and soil moisture observations in groundwater model calibration. *Reviews of Geophysics*, 57(1), 146–182. <https://doi.org/10.1029/2018RG000619>
- Schilling, O. S., Cook, P. G., Grierson, P. F., Dogramaci, S., & Simmons, C. T. (2020). Controls on interactions between surface water, groundwater and riverine vegetation along intermittent rivers and ephemeral streams in arid regions. *Water Resources Research*, e2020WR028429.
- Schilling, O. S., Gerber, C., Partington, D. J., Purtschert, R., Brennwald, M. S., Kipfer, R., et al. (2017). Advancing physically-based flow simulations of alluvial systems through atmospheric noble gases and the novel ³⁷Ar tracer method. *Water Resources Research*, 53(12), 10465–10490. <https://doi.org/10.1002/2017WR020754>
- Schilling, O. S., Parajuli, A., Tremblay Otis, C., Müller, T. U., Antolinez Quijano, W., Tremblay, Y., et al. (2021). Quantifying groundwater recharge dynamics and unsaturated zone processes in snow-dominated catchments via on-site dissolved gas analysis. *Water Research*, 57, e2020WR028479. <https://doi.org/10.1029/2020WR028479>
- Schilling, O. S., Park, Y.-J., Therrien, R., & Nagare, R. M. (2019). Integrated surface and subsurface hydrological modeling with snowmelt and pore water freeze thaw. *Groundwater*, 57(1), 63–74. <https://doi.org/10.1111/gwat.12841>
- Somers, L. D., McKenzie, J. M., Mark, B. G., Lagos, P., Ng, G. H. C., Wickert, A. D., et al. (2019). Groundwater buffers decreasing glacier melt in an Andean watershed but not forever. *Geophysical Research Letters*, 46(22), 13016–13026. <https://doi.org/10.1029/2019GL084730>
- Sprenger, M., Stumpp, C., Weiler, M., Aeschbach, W., Allen, S. T., Benettin, P., et al. (2019). The demographics of water: A review of water ages in the critical zone. *Reviews of Geophysics*, 57(3), 800–834. <https://doi.org/10.1029/2018RG000633>
- Stock, B. C., Jackson, A. L., Ward, E. J., Parnell, A. C., Phillips, D. L., & Semmens, B. X. (2018). Analyzing mixing systems using a new generation of Bayesian tracer mixing models. *PeerJ*, 6, 1–27. <https://doi.org/10.7717/peerj.5096>
- Tang, Q., Schilling, O. S., Kurtz, W., Brunner, P., Vereecken, H., & Hendricks Franssen, H. J. (2018). Simulating flood induced riverbed transience using unmanned aerial vehicles, physically based hydrological modeling, and the ensemble Kalman filter. *Water Resources Research*, 54(11), 9342–9363. <https://doi.org/10.1029/2018WR023067>
- Valder, J. F., Long, A. J., Davis, A. D., & Kenner, S. J. (2012). Multivariate statistical approach to estimate mixing proportions for unknown end members. *Journal of Hydrology*, 460–461, 65–76. <https://doi.org/10.1016/j.jhydrol.2012.06.037>
- Vautier, C., Abhervé, R., Labasque, T., Laverman, A. M., Guillou, A., Chatton, E., et al. (2020). Mapping gas exchanges in headwater streams with membrane inlet mass spectrometry. *Journal of Hydrology*, 581, 124398. <https://doi.org/10.1016/j.jhydrol.2019.124398>. Retrieved from <https://linkinghub.elsevier.com/retrieve/pii/S0022169419311333>
- Von Freyberg, J., Studer, B., & Kirchner, J. W. (2017). A lab in the field: High-frequency analysis of water quality and stable isotopes in stream water and precipitation. *Hydrology and Earth System Sciences*, 21(3), 1721–1739. <https://doi.org/10.5194/hess-21-1721-2017>
- Würsten, M. (1991). *GWB-Hydrogeologische untersuchungen aeschau: Schlussbericht (Technical Report)*. Zurich: Geotechnisches Institut.
- 3M Liqui-Cel. (2017). *A high level of consistency and control*. Germany: Wuppertal. Retrieved from <http://multimedia.3m.com/mws/media/14124850/3m-liqui-cel-membrane-contactors-liquid-degasgasc-1096-pdf>